Estimating the arterial input function from dynamic contrast-enhanced MRI data with compensation for flow enhancement (II)

Applications in spine diagnostics and assessment of crohn's disease

van Schie, Jeroen J.N.; Lavini, Cristina; van Vliet, Lucas J.; Kramer, Gem; Pieters - van den Bos, Indra; Marcus, J. T.; Stoker, Jaap; Vos, Frans M.

DOI
10.1002/jmri.25905

Publication date
2018

Document Version
Final published version

Published in
Journal of Magnetic Resonance Imaging

Estimating the Arterial Input Function From Dynamic Contrast-Enhanced MRI Data With Compensation for Flow Enhancement (II): Applications in Spine Diagnostics and Assessment of Crohn's Disease

Jeroen J.N. van Schie, PhD,[1] Cristina Lavini, PhD,[2] Lucas J. van Vliet, PhD,[1] Gem Kramer, MD,[3] Indra Pieters - van den Bos, MD, PhD,[3] J.T. Marcus, PhD,[3] Jaap Stoker, MD, PhD,[2] and Frans M. Vos, PhD[1,2]*

Background: Pharmacokinetic (PK) models can describe microvascular density and integrity. An essential component of PK models is the arterial input function (AIF) representing the time-dependent concentration of contrast agent (CA) in the blood plasma supplied to a tissue.
Purpose/Hypothesis: To evaluate a novel method for subject-specific AIF estimation that takes inflow effects into account.
Study Type: Retrospective study.
Subjects: Thirteen clinical patients referred for spine-related complaints; 21 patients from a study into luminal Crohn's disease with known Crohn's Disease Endoscopic Index of Severity (CDEIS).
Field Strength/Sequence: Dynamic fast spoiled gradient echo (FSPGR) at 3T.
Assessment: A population-averaged AIF, AIFs derived from distally placed regions of interest (ROIs), and the new AIF method were applied. Tofts' PK model parameters (including v_p and K^{trans}) obtained with the three AIFs were compared. In the Crohn's patients K^{trans} was correlated to CDEIS.
Statistical Tests: The median values of the PK model parameters from the three methods were compared using a Mann–Whitney *U*-test. The associated variances were statistically assessed by the Brown-Forsythe test. Spearman's rank correlation coefficient was computed to test the correlation of K^{trans} to CDEIS.
Results: The median v_p was significantly larger when using the distal ROI approach, compared to the two other methods ($P < 0.05$ for both comparisons, in both applications). Also, the variances in v_p were significantly larger with the ROI approach ($P < 0.05$ for all comparisons). In the Crohn's disease study, the estimated K^{trans} parameter correlated better with the CDEIS ($r = 0.733$, $P < 0.001$) when the proposed AIF was used, compared to AIFs from the distal ROI method ($r = 0.429$, $P = 0.067$) or the population-averaged AIF ($r = 0.567$, $P = 0.011$).
Data Conclusion: The proposed method yielded realistic PK model parameters and improved the correlation of the K^{trans} parameter with CDEIS, compared to existing approaches.
Level of Evidence: 3
Technical Efficacy: Stage 1

J. MAGN. RESON. IMAGING 2018;47:1197–1204.

View this article online at wileyonlinelibrary.com. DOI: 10.1002/jmri.25905

Received Jun 6, 2017, Accepted for publication Oct 16, 2017.

*Address reprint requests to: F.M.V., Lorentzweg 1, Delft, The Netherlands. E-mail: f.m.vos@tudelft.nl

From the [1]Quantitative Imaging Group, Department of Imaging Physics, Delft University of Technology, Delft, The Netherlands; [2]Department of Radiology and Nuclear Medicine, Academic Medical Center, Amsterdam, The Netherlands; and [3]Department of Radiology and Nuclear Medicine, VU University Medical Center, Amsterdam, The Netherlands

Additional supporting information may be found in the online version of this article

Dynamic contrast-enhanced magnetic resonance imaging (DCE-MRI) is an important imaging technique with a wide range of applications. It can be used to study physiological processes involving tissue perfusion in qualitative[1,2] and quantitative[3,4] ways. Several pharmacokinetic (PK) models are available to quantitatively estimate parameters describing microvascular density and integrity.[5] An essential component of PK models is the arterial input function (AIF). The AIF represents the time-dependent concentration of contrast agent (CA) in the blood plasma supplied to the tissue of interest. A correct representation of the AIF is essential for accurate estimation of the PK model parameters.

The AIF is usually obtained by either measuring the concentration from the DCE-MRI data directly, or by using a population-averaged, parametrized model from the literature.[6] When measuring the AIF from the DCE-MRI data, either the full nonlinear relationship between the CA concentration and the MRI signal in an artery close to the tissue of interest is used,[7] or a simplified linear approximation is adopted.[3,8] Generally speaking, a more accurate AIF leads to a more accurate PK analysis.[9,10]

DCE-MRI often uses a fast spoiled gradient echo (FSPGR) sequence, for which a theoretic relationship exists between the CA concentration and the signal enhancement, under the assumption that the magnetization after the repeated application of RF pulses is in a steady state.[11,12] In the case of flowing spins, such as in arterial blood, the assumption of steady state may not hold, as freshly inflowing spins have not received sufficient RF pulses to reach steady state. This effect is particularly evident upstream in larger arteries, where it manifests by a diminished enhancement. This inflow effect introduces a significant bias in the estimation of the AIF, if not accounted for.[13] The influence of flow may be reduced by estimating the AIF in a region distal from the entry point of an artery into the field of view (FOV), yet this may not be sufficient.

We developed an AIF estimation method that models the spin dynamics during the transient state of an FSPGR sequence after contrast agent injection (see Supplementary Material I).

This study aimed to evaluate this novel method in vivo that takes inflow effects into account.

Materials and Methods

Theory

The theoretical treatment of the flow correction estimation method is explained in Supplementary Materials I.

Patients

Two separate datasets were used for evaluation purposes. The first dataset was obtained from 13 clinical patients who were referred for an MRI using a contrast agent for variety of spine-related complaints. All these patients were consecutively included in the frame of a DCE-MRI protocol optimization study. The second dataset was from 21 consecutive patients from a recently concluded prospective study into luminal Crohn's disease. Ileocolonoscopy was performed within 2 weeks of the MRI scan by a gastroenterologist. The endoscopist applied the Crohn's Disease Endoscopic Index of Severity (CDEIS) to assess endoscopic disease activity. The local Medical Ethics Committee approved both studies. All patients had given informed consent to usage of their data.

MRI Acquisition Protocols

DCE-MR imaging was performed with FSPGR sequences on two 3.0T scanners in two different medical centers (VUMC Amsterdam and AMC Amsterdam): Philips Ingenuity for the spine patients and Philips Ingenia for the Crohn's patients (both scanners were from Philips, Best, The Netherlands). Care was taken that the descending aorta was clearly visible in all acquired data.

In the first dataset, the scans were made with a range of settings, to explore the method's ability to obtain an AIF under various conditions. The scan parameters of the 3D acquisition were: sagittal orientation, matrix size: 256 × 256 × (4–6) voxels, FOV: 320 × 320 × (16.0–22.5) mm^3, T_R = (3.2–4.3) msec, T_E = (1.4–2.7) msec, α = (10–15) degrees, no partial Fourier, no parallel imaging excepting one case, temporal resolutions of (4.26–7.51) seconds, for a total scan time of (213–376) seconds ([50–70] volumes). After ~30 seconds, a bolus injection of gadoterate meglumine (Dotarem 0.5 mmol/ml; Guerbet; Roissy; France) was administered intravenously, at a rate of 3 ml/s, for a total dose of 0.1 mmol/kg body mass, followed by a 20-ml saline flush at a rate of 5 ml/s.

In the second dataset, all scans were made with identical settings (coronal orientation, matrix size: 224 × 224 × 20 voxels, FOV: 400 × 400 × 50 mm^3, TR = 2.86 msec, TE = 1.80 msec, $\alpha = 15°$, no partial Fourier, no parallel imaging) with a temporal resolution of 1.27 seconds, for a total scan time of 381 seconds (300 volumes). After ~1 minute, a bolus injection of gadobutrol (Gadovist 1.0 mmol/ml; Schering, Berlin, Germany) was administered intravenously, at a rate of 5 ml/s, for a total dose of 0.1 mmol/kg body mass, followed by a saline flush.

Artery Selection and AIF Estimation

The first step in estimating the AIF from a DCE-MRI dataset was to segment the aorta and iliac arteries. In the first dataset, the lower temporal resolution and higher degree of noise necessitated a manual segmentation. This was done by delineating regions through manually drawn polygons. In the second dataset, an automatic segmentation method was applied. This automatic segmentation method was based on an empiric approach relying on two properties of the data: the time to peak is relatively short, and there is a marked change in intensity. The segmentation method is described in detail in Supplementary Material II.

Next, a signal-ratio curve was computed in each voxel from the segmented region, by dividing the measured signal by the average precontrast signal (see Supplementary Material II). From each signal-ratio curve, the corresponding number of pulses n was computed, and, with the number of pulses known, time–concentration

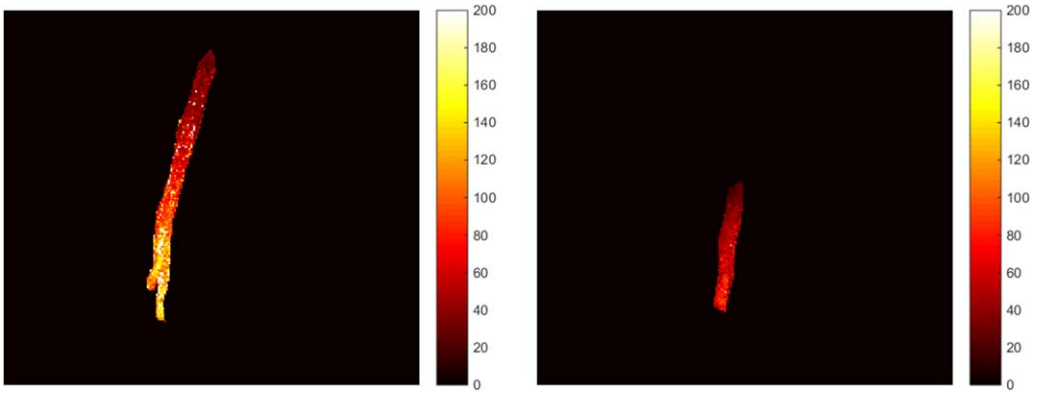

FIGURE 1: Maximum intensity projections of *n*-maps in the sagittal direction of two subjects from the spine study. The arteries were segmented manually.

curves (TCCs) were computed. (See Supplementary Material I, or Part I of this article.)

After all the TCCs were computed, they were aligned with each other based on the estimated time shift (see Supplementary Material II), while using linear interpolation. Since the distribution of the estimated concentrations at a given timepoint is skewed, the mode of the data at each timepoint was chosen as the best estimate for the concentration. The mode was computed using a mean-shift procedure with a Gaussian kernel.[14] Furthermore, the full width at half maximum was chosen as the measure of uncertainty.

The proposed method was compared to an approach in which a TCC was computed from a small, manually drawn region of interest (ROI) in the iliac artery, distal from the entry point of the aorta into the FOV. The concentration was computed from the MRI signal in these ROIs while assuming an infinite number of pulses, as is done traditionally.[13] Furthermore, the AIF from the proposed method was compared to the population averaged, parameterized AIF presented by Orton et al.[15]

Pharmacokinetic Analysis

For each DCE-MRI acquisition of the first dataset, an ROI was manually drawn inside vertebra considered healthy by a radiologist (I.P., 10 years of experience). From these ROIs, time intensity curves (TICs) were extracted and averaged. These TICs were then converted to TCCs, using the same method as described above, but setting the number of pulses to infinity. This is allowed, since the ROIs were constantly inside the FOV, and the magnetization was therefore in the steady state. The T_{10} time of the bone tissue was set to 586 msec.[16]

For each acquisition of the second dataset, the volumes at each timepoint were registered to each other using the method of Li et al,[17] to compensate for motion of the tissue. Subsequently, regions presenting active Crohn's disease were identified by an expert abdominal radiologist (J.S.). The presence of active Crohn's disease was based on other available MRI sequences. A research fellow delineated each such region as instructed by the radiologist. TICs were extracted from these ROIs, averaged, and converted to TCCs. In the absence of a literature value for the T_{10}-time of bowel tissue, the T_{10}-time was set to 700 msec.

The PK properties of the investigated tissues were determined using Tofts' extended two-compartment PK model.[5] Here, the tissue concentration is modeled as a function of the plasma concentration $C_p = AIF/(1 - Hct)$, as well as the volume fractions of plasma (v_p), interstitial space (v_e), and the transfer rate coefficient (k_{ep}). These factors were estimated numerically by fitting Tofts' model to the measured TCC in the tissue, using least-squares regression. The hematocrit value *Hct* was set to 0.42. The

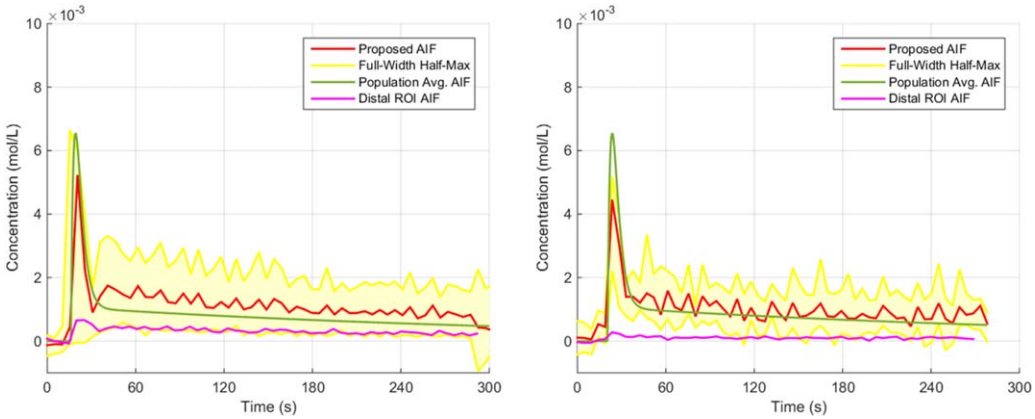

FIGURE 2: AIFs of two subjects of the spine study, obtained with the proposed method (red), also showing the associated full-width at half-maximum intervals (yellow). AIFs obtained with the distal ROI method (magenta) and Orton's population-averaged AIF (green) are plotted for comparison.

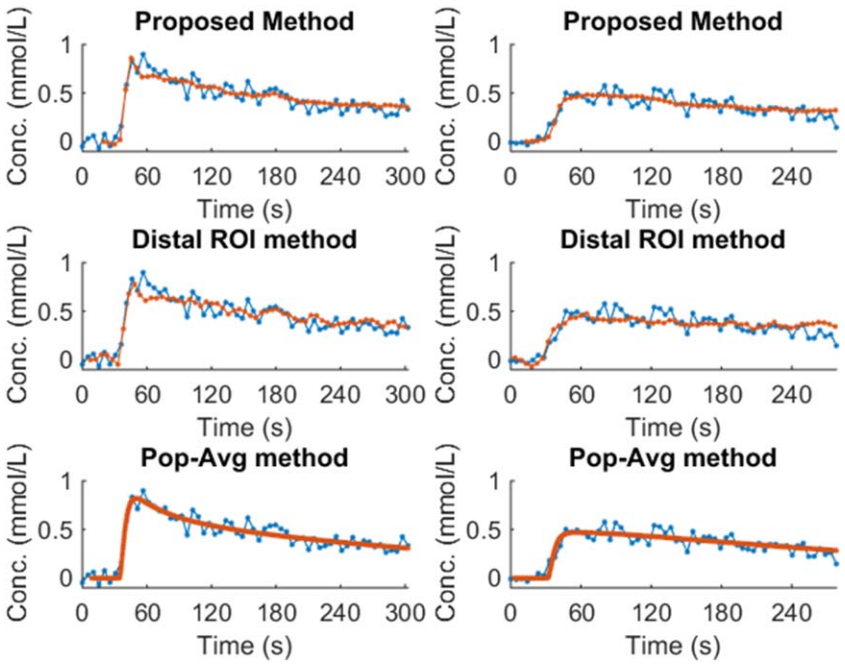

FIGURE 3: Fits of modeled time–concentration curves (red) to the measured time–concentration curves (blue) in vertebra of subjects of the spine study. The results of two subjects are shown columnwise. AIFs obtained with the proposed method (top row), distal ROI method (middle row), and population-average method (bottom row) were used as input to the PK model.

procedure was performed for the patients of both datasets, with AIFs obtained using all three methods described. The root mean square errors (RMSEs) of the fits averaged over all patients were compared to assess the appropriateness of the methods. This was done using Student's *t*-test. The median values of the PK model parameters obtained with the three methods were compared using a Mann–Whitney *U*-test. The associated variances were statistically assessed by the Brown-Forsythe test. Finally, the volume transfer coefficients $K^{trans} = v_e \cdot k_{ep}$ were computed for the patients of the second dataset, and compared to the CDEIS score of each patient. Spearman's rank correlation coefficient was computed for each AIF extraction method, as an indirect, quantitative measure of the usefulness of the methods. $P < 0.05$ was considered statistically significant in all the statistical tests.

Results

Results From the Spine Data

In the dataset of the 13 spine patients, the quality of the arterial signal was very heterogeneous, ranging from TICs with a pronounced peak to others with an almost invisible peak. These acquisitions were processed according to the proposed method. The estimated number of pulses in each segmented voxel was mapped back into a volume to produce an '*n*-map' of each dataset. Maximum intensity projections along the sagittal direction of two representative *n*-maps are shown in Fig. 1. Note that the number of pulses increases from top to bottom, corresponding to the direction of the blood flow.

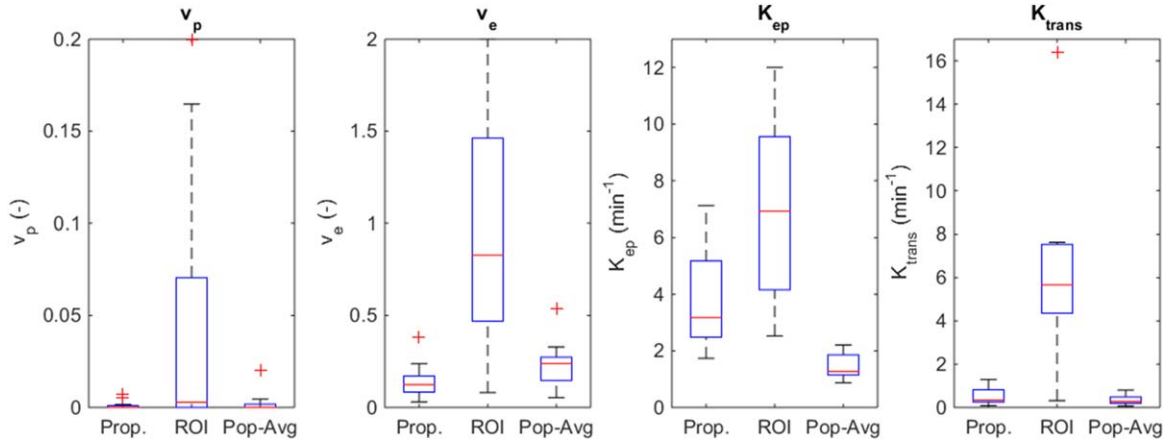

FIGURE 4: Boxplots showing the distributions of estimated PK parameters. The red lines represent the medians while the blue boxes reflect the 25th to 75th percentile ranges; whiskers extend to the most extreme value inside 1.5 times the interquartile range; values outside these ranges are indicated as individual points.

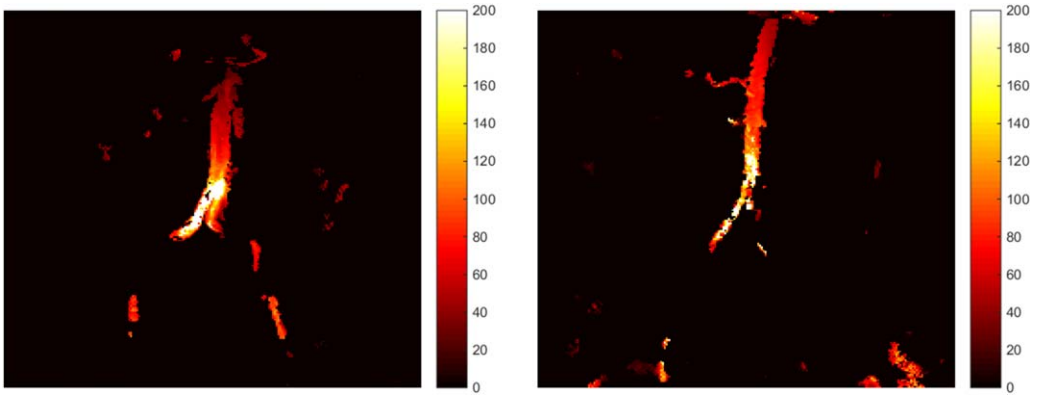

FIGURE 5: Crohn's patients study, coronal acquisition. Maximum intensity projections of *n*-maps of two representative datasets, showing the estimated number pulses in the segmented voxels. The segmentations were done automatically.

Two representative modal AIFs, estimated using the two *n*-maps of Fig. 1, are shown in Fig. 2. Also, the AIFs estimated using the ROI method (assuming infinite pulses), as well as Orton et al's population-averaged AIF, is shown in the same graphs.

The AIFs were used in the fitting of Tofts' model to the TCCs in the bone marrow. The results of using the AIFs of the three methods as input is shown in Fig. 3. No significant differences were found between the average RMSEs of the three AIF estimation methods ($P > 0.05$). The distributions of the estimated PK parameters of all subjects in this dataset are shown as a boxplot in Fig. 4. There was a significantly larger variance in the estimations of all four parameters by means of the distal ROI method, compared to the other methods ($P < 0.05$ for all comparisons). Furthermore, the distal ROI approach yielded unrealistic estimations ($v_e > 1$) in several cases.

Results From the Crohn's Disease Data

Maximum intensity projections in the coronal direction of the computed *n*-maps of two representative patients are shown in Fig. 5. The modal AIFs corresponding to the *n*-maps of Fig. 5 are shown in Fig. 6. The AIFs estimated with the distal ROI method and the population-averaged AIF are also shown for comparison.

Fitting of the Tofts' model to the TCCs of bowel tissue in two subjects of the Crohn's disease data, using AIFs obtained with each of the three methods, is shown in Fig. 7. The differences in average RMSE between the three methods are not significant ($P > 0.49$). The distributions of the estimated PK parameters of all subjects in this dataset are shown as a boxplot in Fig. 8. There was a significantly higher median and larger variance in the estimations of v_p by means of the distal ROI method, compared to the other methods ($P < 0.05$ in all comparisons).

Further results of the PK analysis are shown in Fig. 9. Here the estimated K^{trans} parameters are plotted against the CDEIS scores, for each of the three methods. Linear fits are drawn with red lines. CDEIS scores were unavailable for two subjects because the affected area could not be inspected by the gastroenterologist due to strictures in the bowel. Hence, the Spearman's rank correlation coefficients were computed for $N = 19$ subjects. A strong correlation of $r = 0.733$ ($P < 0.001$) was found when using the proposed method using an inflow-corrected AIF, while moderate correlations were found for the method using an AIF from a

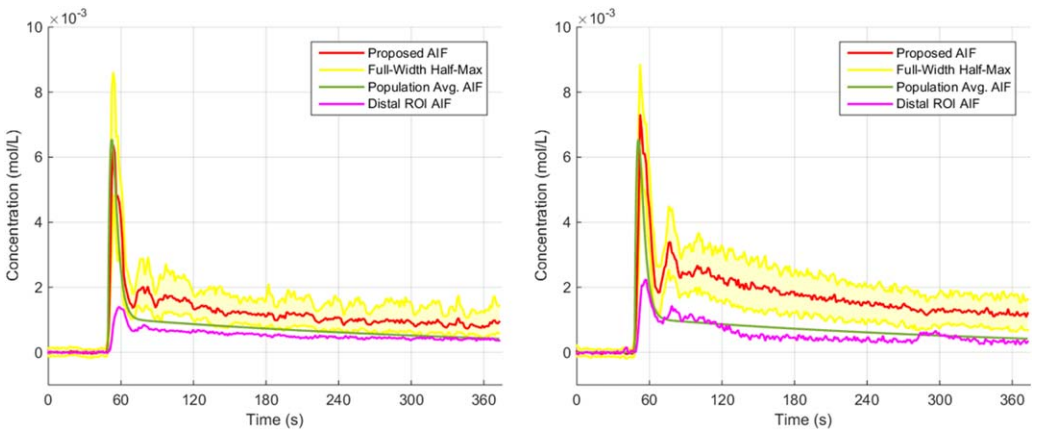

FIGURE 6: Two estimated AIFs determined for the same patients as in Fig. 5. Red: Modal estimated AIF; Yellow: Full-width at half-maximum; Green: Orton's population-average AIF; Magenta: AIF estimated with the distal ROI method.

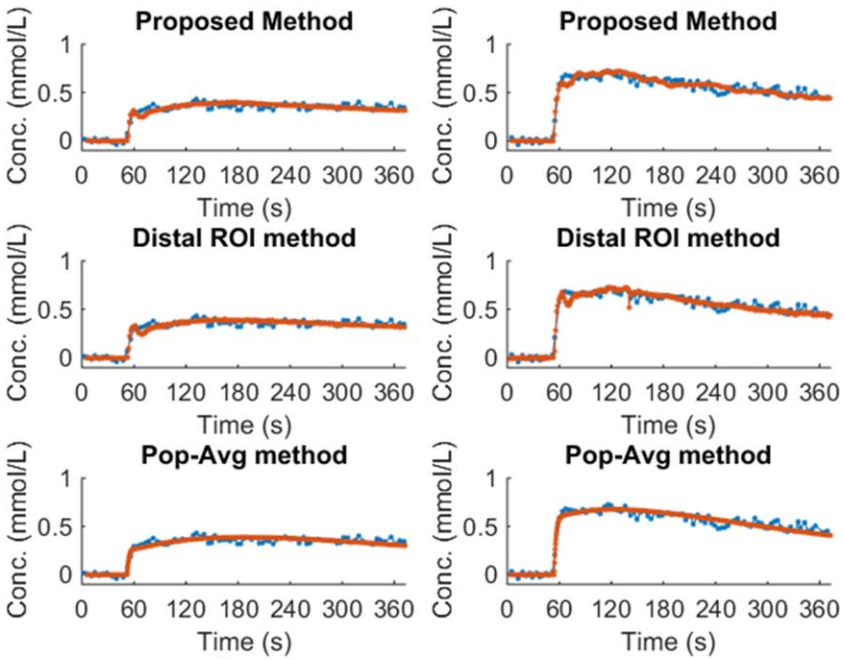

FIGURE 7: Tofts' model fitted to the measured time–concentration curves of two subjects of the Crohn's disease study. Measured (blue) and modeled (red) time–concentration curves in bowel tissue, using AIFs from the proposed (top), distal ROI (middle), and population-averaged (bottom) methods.

manually drawn ROI ($r = 0.429$, $P = 0.067$) and the population averaged AIF ($r = 0.567$, $P = 0.011$).

Discussion

The results of this patient study show that the proposed method can estimate AIFs from DCE-MRI scans with a variety of scan settings, even when inflow effects are severe. The reconstructed bolus peaks were clearly visible, and resemble those of the population-averaged AIF. This resemblance is expected, since the estimation of the number of pulses in each voxel relies on the area under the bolus peak, which is constrained to that of the population average.

The three AIFs extracted in different ways produced equally good fits of the PK models, but different model parameters. This underlines the importance of a correct AIF estimation procedure. While the AIFs obtained from a distal part of the aorta yielded unrealistic parameters, this was not the case with our approach. Unfortunately, the absence of a gold standard for AIF and K model estimation hinders the interpretation of the extracted parameters.

In both patient studies, the concentrations in the slowly decaying part of the AIFs (the "tails"), as estimated with the proposed method, were slightly higher than those estimated with the other two methods. This is a result of the constraint imposed on the area under the bolus peak in the estimation of the number of pulses. The effect can be especially recognized in signal-ratio curves presenting a low bolus peak. Implicitly, the low bolus peak is assumed to be caused by the inflow

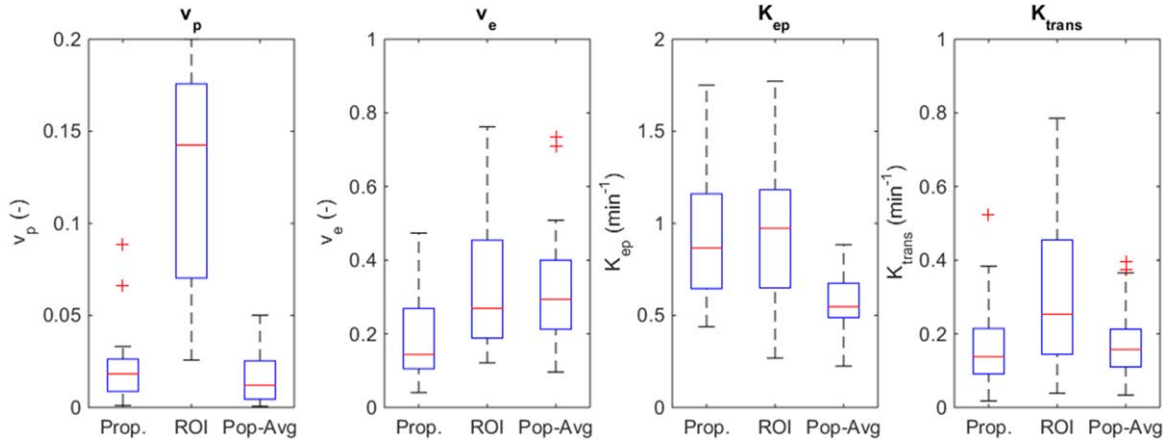

FIGURE 8: Boxplots showing the distributions of estimated PK parameters. The red lines represent the medians while the blue boxes reflect the 25th to 75th percentile ranges; whiskers extend to the most extreme value inside 1.5 times the interquartile range; values outside these ranges are indicated as individual points.

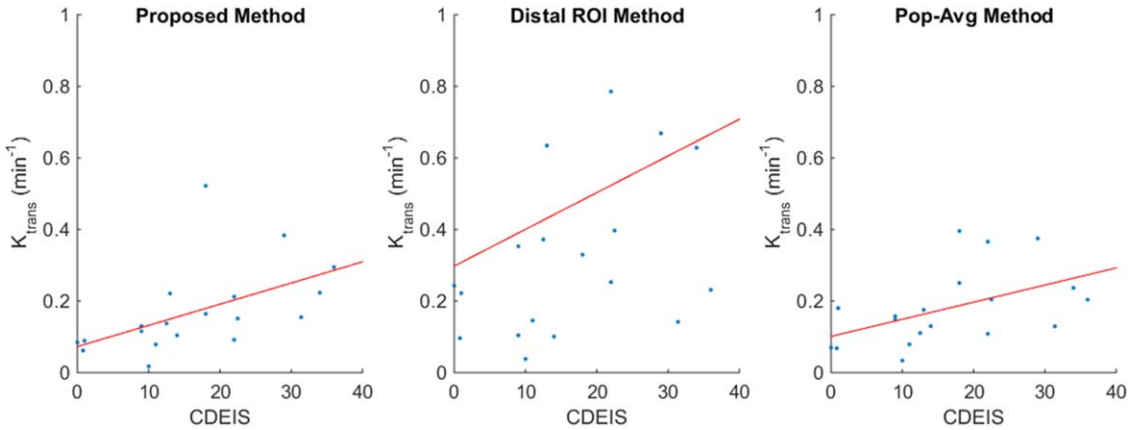

FIGURE 9: Result of the pharmacokinetic analyses of the second dataset. K_{trans} is plotted against the CDEIS score. Left: proposed method. Middle: ROI method. Right: population average method. The red lines are linear fits.

effect, and accordingly, the estimated number of pulses will be low. This leads to a higher estimated concentration in both the peak and the tail. Still, the theoretical signal ratio for the estimated concentrations at any given timepoint matched the measured signal ratios in the artery, which means that the estimated concentration is accurate.

Crohn's disease is associated with altered vascularization.[18] As such, the K^{trans} parameter might reflect an important aspect of the pathology. However, the disease has a very complex etiology. K^{trans} could contribute to the characterization of the disease, in combination with other parameters.

Importantly, K^{trans} is a physical property of a tissue's microstructure. It is calculated based on the inflowing contrast agent concentration, which is (in turn) computed based on the tissue's T_1 value. A careful calibration of a tissue's T_1 value (for instance, by performing a Look–Locker sequence[19] could facilitate its standardization across different scanners, and hence clinical centers. The improved correlation between CDEIS and the K^{trans} extracted with the proposed technique may suggest that it enables better assessment of Crohn's disease severity compared to the other AIF methods.

While it is recognized that a patient-specific AIF improves the quality of PK model analysis,[20,21] obtaining a reliable AIF remains a challenge. Factors such as incomplete signal saturation due to flow or T_2^* decay can result in a reduced magnitude of the first AIF peak.[22,23] It is well known that this effect depends on the location where the artery is sampled with respect to the imaging volume.[20,24] In the aorta, where flow is significant and high concentrations of Gd prevail, the first-pass peak can disappear altogether.[25,26]

Alternative methods that correct for flow include the reference region model AIF[27] or the phase-based AIF approach.[28] Our method is different in that it specifically addresses the flow and T_2^* saturation artifacts. Its reliance on a priori knowledge (in our case the assumption on the shape and area under the curve of the AIF) is a common feature of many correction and AIF estimation models. Other examples are in the angulation of the phase-based AIF[28] and the (muscle) PKM parameters in the reference region model.[27]

Recently, Wang et al[23] pointed out how a low dosage of Gd can effectively produce an AIF showing a clear peak, as a result of the lower T_2^* reduction. A possible further development of our method would be to apply it to low-dose AIF, as this could help separate T_2^* effects from flow effects

A limitation of the proposed method is its dependence on the presence of a bolus peak. If the bolus peak is entirely not visible in the original DCE-MRI data, the number of pulses, and therefore the AIF, cannot be estimated reliably. In that case, it becomes impossible to precisely estimate the model parameters, such as the position of the bolus peak. This may occur, for example, when the temporal resolution is too low, and the bolus peak occurs between two timepoints. Furthermore, the method relies on a proper segmentation of the artery. If the automated segmentation method wrongly includes regions outside the artery, the estimated TCCs at these locations may be unreliable. This is because the bolus peak becomes less well visible if a constant signal is mixed with the true AIF signal. A manual segmentation could be helpful in some cases, although this might not be desirable.

Some limitations of our experiment in the Crohn's disease data relate to the limited number of patients and the annotation by one radiologist. As such, the outcome should be considered an indication of the improved reliability of our method compared to the conventional approaches. Also, we have not addressed the problem of incomplete spoiling, and incorrect RF as done by Garpebring et al,[13] or by B_1 inhomogeneity or partial volume effects.[29] It possible that inclusion of this effect might change our results.

Finally, the most important limitation is the lack of a reference standard. Obtaining a true TCC of contrast agent

in flowing blood under realistic measurement circumstances is a highly complex, still unsolved issue.

In conclusion, we applied a new subject-specific AIF estimation method to two patient cohorts in order to study the merit of correcting for flow enhancement. With the spine dataset, we demonstrated that our approach resulted in realistic PK model parameters, while applying a range of scan settings. Using the Crohn's disease dataset, we showed that our method facilitates significant correlation of K^{trans} with CDEIS. What's more, our subject-specific approach yielded significantly higher correlation than a method relying on a population-average AIF. Other applications of PK modeling may also benefit from our method.

Acknowledgment

Contract grant sponsor: European Union's Seventh Framework Programme; contract grant number: FP7/2007-2013; VIGOR++ Project that was sponsored through the EU's 7th framework programme; contract grant number: 270379.

References

1. Hemke R, Lavini C, Nusman CM, et al. Pixel-by-pixel analysis of DCE-MRI curve shape patterns in knees of active and inactive juvenile idiopathic arthritis patients. Eur Radiol 2014;24:1686–1693.
2. Chen WT, Shih TT, Chen RC, et al. Vertebral bone marrow perfusion evaluated with dynamic contrast-enhanced MR imaging: significance of aging and sex. Radiology 2001;220:213–218.
3. Zollner FG, Zimmer F, Klotz S, Hoeger S, Schad LR. Renal perfusion in acute kidney injury with DCE-MRI: deconvolution analysis versus two-compartment filtration model. Magn Reson Imaging 2014;32:781–785.
4. Lim SW, Chrysochou C, Buckley DL, Kalra PA, Sourbron SP. Prediction and assessment of responses to renal artery revascularization with dynamic contrast-enhanced magnetic resonance imaging: a pilot study. Am J Physiol Renal Physiol 2013;305:F672–678.
5. Tofts PS, Brix G, Buckley DL, et al. Estimating kinetic parameters from dynamic contrast-enhanced T(1)-weighted MRI of a diffusable tracer: standardized quantities and symbols. J Magn Reson Imaging 1999;10:223–232.
6. Parker GJ, Roberts C, Macdonald A, et al. Experimentally-derived functional form for a population-averaged high-temporal-resolution arterial input function for dynamic contrast-enhanced MRI. Magn Reson Med 2006;56:993–1000.
7. Jensen RL, Mumert ML, Gillespie DL, Kinney AY, Schabel MC, Salzman KL. Preoperative dynamic contrast-enhanced MRI correlates with molecular markers of hypoxia and vascularity in specific areas of intratumoral microenvironment and is predictive of patient outcome. Neuro Oncol 2014;16:280–291.
8. Taouli B, Johnson RS, Hajdu CH, et al. Hepatocellular carcinoma: perfusion quantification with dynamic contrast-enhanced MRI. AJR Am J Roentgenol 2013;201:795–800.
9. Rijpkema M, Kaanders JH, Joosten FB, van der Kogel AJ, Heerschap A. Method for quantitative mapping of dynamic MRI contrast agent uptake in human tumors. J Magn Reson Imaging 2001;14:457–463.
10. Aronhime S, Calcagno C, Jajamovich GH, et al. DCE-MRI of the liver: effect of linear and nonlinear conversions on hepatic perfusion quantification and reproducibility. J Magn Reson Imaging 2014;40:90–98.
11. Fram EK, Herfkens RJ, Johnson GA, et al. Rapid calculation of T1 using variable flip angle gradient refocused imaging. Magn Reson Imaging 1987;5:201–208.
12. Stalder AF, von Elverfeldt D, Paul D, Hennig J, Markl M. Variable echo time imaging: Signal characteristics of 1-M gadobutrol contrast agent at 1.5 and 3T. Magn Reson Med 2008;59:113–123.
13. Garpebring A, Wirestam R, Ostlund N, Karlsson M. Effects of inflow and radiofrequency spoiling on the arterial input function in dynamic contrast-enhanced MRI: a combined phantom and simulation study. Magn Reson Med 2011;65:1670–1679.
14. Cheng YZ. Mean shift, mode seeking, and clustering. IEEE Trans Pattern Anal Mach Intel 1995;17:790–799.
15. Orton MR, d'Arcy JA, Walker-Samuel S, et al. Computationally efficient vascular input function models for quantitative kinetic modelling using DCE-MRI. Phys Med Biol 2008;53:1225–1239.
16. de Bazelaire CM, Duhamel GD, Rofsky NM, Alsop DC. MR imaging relaxation times of abdominal and pelvic tissues measured in vivo at 3.0 T: preliminary results. Radiology 2004;230:652–659.
17. Li Z, Tielbeek JA, Caan MW, et al. Expiration-phase template-based motion correction of free-breathing abdominal dynamic contrast enhanced MRI. IEEE Trans Biomed Eng 2015;62:1215–1225.
18. Danese S, Sans M, de la Motte C, et al. Angiogenesis as a novel component of inflammatory bowel disease pathogenesis. Gastroenterology 2006;130:2060–2073.
19. Look DC, Locker DR. Time saving in measurement of NMR and EPR relaxation times. Rev Sci Instrum 1970;41:250–251.
20. Port RE, Knopp MV, Brix G. Dynamic contrast-enhanced MRI using Gd-DTPA: Interindividual variability of the arterial input function and consequences for the assessment of kinetics in tumors. Magn Reson Med 2001;45:1030–1038.
21. O'Connor JPB, Jackson A, Parker GJM, Jayson GC. DCE-MRI biomarkers in the clinical evaluation of antiangiogenic and vascular disrupting agents. Br J Cancer 2007;96:189–195.
22. Gatehouse PD, Elkington AG, Ablitt NA, Yang G-Z, Pennell DJ, Firmin DN. Accurate assessment of the arterial input function during high-dose myocardial perfusion cardiovascular magnetic resonance. J Magn Reson Imaging 2004;20:39–45.
23. Wang S, Fan X, Medved M, et al. Arterial input functions (AIFs) measured directly from arteries with low and standard doses of contrast agent, and AIFs derived from reference tissues. Magn Reson Imaging 2016;34:197–203.
24. Hodgson RJ, Connolly S, Barnes T, Eyes B, Campbell RSD, Moots R. Pharmacokinetic modeling of dynamic contrast-enhanced MRI of the hand and wrist in rheumatoid arthritis and the response to anti-tumor necrosis factor-α therapy. Magn Reson Med 2007;58:482–489.
25. Wang H, Cao Y. Correction of arterial input function in dynamic contrast-enhanced MRI of the liver. J Magn Reson Imaging 2012;36:411–421.
26. Dutoit JC, Vanderkerken MA, Verstraete KL. Value of whole body MRI and dynamic contrast enhanced MRI in the diagnosis, follow-up and evaluation of disease activity and extent in multiple myeloma. Eur J Radiol; 82:1444–1452.
27. Yankeelov TE, Cron GO, Addison CL, et al. Comparison of a reference region model with direct measurement of an AIF in the analysis of DCE-MRI data. Magn Reson Med 2007;57:353–361.
28. Garpebring A, Wirestam R, Yu J, Asklund T, Karlsson M. Phase-based arterial input functions in humans applied to dynamic contrast-enhanced MRI: potential usefulness and limitations. MAGMA 2011;24:233–245.
29. Cheng HL. T1 measurement of flowing blood and arterial input function determination for quantitative 3D T1-weighted DCE-MRI. J Magn Reson Imaging 2007;25:1073–1078.